

Structure Based Design, Synthesis, Pharmacophore Modeling, Virtual Screening, and Molecular Docking Studies for Identification of Novel Cyclophilin D Inhibitors

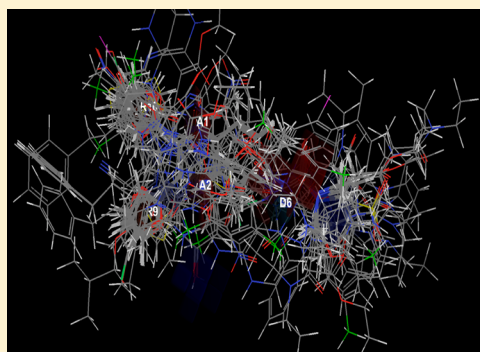
Koteswara Rao Valasani,[†] Jhansi Rani Vangavaragu,[†] Victor W. Day,[‡] and Shirley ShiDu Yan^{*,†}

[†]Department of Pharmacology & Toxicology and Higuchi Bioscience Center, School of Pharmacy, University of Kansas, Lawrence, Kansas 66047, United States

[‡]Department of Chemistry, University of Kansas, Lawrence, Kansas 66045, United States

S Supporting Information

ABSTRACT: Cyclophilin D (CypD) is a peptidyl prolyl isomerase F that resides in the mitochondrial matrix and associates with the inner mitochondrial membrane during the mitochondrial membrane permeability transition. CypD plays a central role in opening the mitochondrial membrane permeability transition pore (mPTP) leading to cell death and has been linked to Alzheimer's disease (AD). Because CypD interacts with amyloid beta ($A\beta$) to exacerbate mitochondrial and neuronal stress, it is a potential target for drugs to treat AD. Since appropriately designed small organic molecules might bind to CypD and block its interaction with $A\beta$, 20 trial compounds were designed using known procedures that started with fundamental pyrimidine and sulfonamide scaffolds known to have useful therapeutic effects. Two-dimensional (2D) quantitative structure–activity relationship (QSAR) methods were applied to 40 compounds with known IC_{50} values. These formed a training set and were followed by a trial set of 20 designed compounds. A correlation analysis was carried out comparing the statistics of the measured IC_{50} with predicted values for both sets. Selectivity-determining descriptors were interpreted graphically in terms of principle component analyses. These descriptors can be very useful for predicting activity enhancement for lead compounds. A 3D pharmacophore model was also created. Molecular dynamics simulations were carried out for the 20 trial compounds with known IC_{50} values, and molecular descriptors were determined by 2D QSAR studies using the Lipinski rule-of-five. Fifteen of the 20 molecules satisfied all 5 Lipinski rules, and the remaining 5 satisfied 4 of the 5 Lipinski criteria and nearly satisfied the fifth. Our previous use of 2D QSAR, 3D pharmacophore models, and molecular docking experiments to successfully predict activity indicates that this can be a very powerful technique for screening large numbers of new compounds as active drug candidates. These studies will hopefully provide a basis for efficiently designing and screening large numbers of more potent and selective inhibitors for CypD treatment of AD.



1. INTRODUCTION

Alzheimer's disease (AD) is the most common cause of dementia in adults, resulting in a disorder of cognition and memory due to neuronal stress and eventuating in cell death. Current research indicates that mitochondrial and synaptic dysfunction is an early pathological feature of an AD affected brain.^{1–5} Mitochondrial amyloid- β ($A\beta$) accumulation in synaptic mitochondria has been shown to impair mitochondrial structure and function. $A\beta$ accumulation also has been shown to influence calcium homeostasis, energy metabolism, membrane potential, membrane permeability transition pore (mPTP), mitochondrial dynamics, respiration, and oxidative stress.^{6–11} Preventing and/or halting AD at its earliest stages may be possible by suppressing $A\beta$ -induced mitochondrial toxicity.¹² Blocking $A\beta$ production or developing $A\beta$ inhibitors are two possible approaches. Other strategies might include developing inhibitors that block the clipping action of secretases,^{13–20} compounds that interfere with $A\beta$ oligomeriza-

tion,^{21–23} and “passive vaccines” designed to clear amyloid directly.¹³ To date, none of these approaches have been shown to dramatically improve AD symptoms or protect brain cells and no drugs have entered clinical trials due to concerns about side effects. Because AD is a multifaceted disease and its molecular biology is poorly understood, multitargeted approaches for AD treatment should be more effective.

Cyclophilin D (CypD), a peptidyl prolyl isomerase F, resides in the mitochondrial matrix and associates with the inner mitochondrial membrane during the mitochondrial membrane permeability transition. CypD plays a central role in opening the mPTP leading to cell death. The level of CypD was significantly elevated in neurons in AD-affected regions. We have shown that CypD forms a complex with $A\beta$ (CypD– $A\beta$) that is present in the cortical mitochondria of AD brain and

Received: January 11, 2014

Published: February 20, 2014

transgenic mice overexpressing human mutant form of amyloid precursor protein and $A\beta$ (Tg mAPP). Surface plasmon resonance (SPR) has been used to show a high binding of recombinant CypD protein to $A\beta$. When CypD was not present, $A\beta$ -mediated mitochondrial and synaptic dysfunction was reduced.^{6,24} Although the precise role of $A\beta$ in mitochondria is not yet defined, reports illustrate that an interaction between mitochondrial $A\beta$ and mitochondrial proteins, such as CypD, exacerbates mitochondrial and neuronal stress in transgenic AD mouse models.^{6,8,24,25} These reports support the use of CypD a potential target for drug development in the treatment of AD. Blockade of CypD protects against $A\beta$ - and oxidative stress-induced mitochondrial and synaptic degeneration and improves mitochondrial and cognitive function. To date, the most specific inhibitor of the mPTP is cyclosporin A (CsA), which acts by inhibiting the peptidyl-prolyl cis–trans isomerase (PPIase) activity of CypD.^{26–28} Unfortunately, CsA lacks clinical significance because of its immunosuppressive effect by inhibiting calcinurin (a calcium dependent protein phosphatase) and its inability to pass through the blood–brain barrier (BBB). Several CsA derivatives have therefore been developed, including *N*-Me-Ala-6-cyclosporin A and *N*-Me-Val-4-cyclosporin, which both lack the unfavorable immunosuppressive effects but are still potent inhibitors of PPIase activity of CypD, thereby antagonizing mPTP opening and apoptosis induction.^{29,30} Recently, Sanglifehrin A (SfA) and antamanide (AA) have been produced for inhibition of mPTP but lack significance as therapeutic molecules due to severe side effects including neurotoxicity, hepatotoxicity, nephrotoxicity, and poor permeability through the BBB.^{31,32} Although Guo et al. have synthesized small molecule quinoxaline derivatives that inhibit the calcium-induced mPTP opening,³³ their effects on mPTP require re-evaluation. Other currently available CypD inhibitors have disadvantages, such as low solubility, poor infiltration of the blood–brain barrier, high toxicity, and low cell permeability.

The present study constructed a 2D quantitative structure–activity relationship (QSAR) and 3D ligand-based pharmacophore model from a training set of 40 compounds. This training set was then used to predict the inhibitory activity of a test set of 20 newly designed molecules. Validity of the QSAR model was indicated by linearity of the correlation, root-mean-square error (RMSE), and the correlation factor (R^2). The pharmacophore model was used to select hits for docking studies from the test set. The docking studies of test set inhibitors with CypD were carried out to determine their binding affinity differences. Reliable models with respect to binding affinity and compound selectivity discrimination were obtained in this manner. Here, we report the design, synthesis, characterization (including three crystal structure determinations), and modeling studies for novel small-molecule CypD inhibitors based on new 4-aminobenzenesulfonamide and tetrahydropyrimidine scaffolds. Molecular docking can be used to interpret the efficacy of the novel molecules to inhibit CypD PPIase activity and hopefully indicate those that may be useful as drugs for the treatment and management of AD.

2. MATERIALS AND METHODS

In silico Study. All in silico studies were performed using Molecular Operating Environment (MOE), MOE2013.08.

QSAR Study. The 3D models were built for all the compounds, and the energy was minimized to a root mean square (RMS) gradient of 0.01 kcal/mol and an RMS distance

of 0.1 Å. MOE 2D-QSAR models were utilized for the 20 newly designed molecules, and these are the *test* compounds. A previously reported set of 40 molecules was used as the *training* set.^{34–36} The QSAR model was constructed for the *training* set of 40 compounds from their predicted QSAR descriptors (SlogP, density, molar refractivity, molecular weight, atomic polarizability, logP(o/w), logS, polar surface area, van der Waals volume, and radius of gyration). The \$PRED descriptor was considered as a dependent variable and activity field; the remaining descriptors are independent. Regression analysis was conducted and performed; the RMSE and R^2 values were derived from the fit of \$PRED values vs SlogP. This QSAR model was applied to validate and evaluate the predicted activities and the residuals of the training set.

A correlation plot was constructed taking the predicted (\$PRED) values on (*X*-axis) and the predicted IC_{50} activities on (*Y*-axis). The outliers showing the *Z*-score above 1.5 are eliminated from this plot. The predicted (\$PRED) values of the 20 test set compounds were evaluated using the QSAR fit constructed from training set QSAR model. RMSE and R^2 values were defined for the test set compounds by performing regression analysis. All the descriptors were subjected to pruning, and the optimum set of molecules was selected. The “QuaSAR-Contingency” application of MOE was used to identify the best molecules in the data set. A graphical 3D scatter plot was constructed from the first three principal components (PCA1, PCA2, and PCA3).

Pharmacophore Generation. A Pharmacophore model was generated where the databases of 3D conformations was filtered based on the positions of annotation points derived from each of the conformations. A pharmacophore query was created from the training set molecules by considering annotation points such as aromatic center, H-bond donors and acceptors, and hydrophobic centroids of the molecule. This query was searched against the database of test set molecules to identify the similar pharmacophore model among them and separate the active compounds from the rest of the database. After the primary search, the query was subjected to refinement by excluding the external volumes that were not matching to the query and eliminating them from the search. The test data set conformations found to be having similar pharmacophore models were aligned for clear visualization.

Molecular Docking with CypD.^{37,38} *Preparation of CypD Protein.* The 3D coordinates of CypD were obtained from Protein Data Bank (PDB ID: 2BIT) and loaded into MOE. The water molecules and heteroatoms were eliminated, and polar hydrogens were added. A temperature of 300 K, and salt concentration of 0.1 and pH 7 was specified in implicit solvated environment to carry out the protonation process. Then, the structure was energy-minimized in the MMFF94x force field to an RMS gradient of 0.05. The energy minimized conformation of CypD was then subjected to a 10 ns molecular dynamic simulations at a constant temperature of 300 K, heat time of 10 ps, and temperature relaxation of 0.2 ps.

The CypD structure was searched against the Blast-P similarity search tool against the PDB and the similar binding domains were identified. The identified residues (residues His 54, Arg 55, Phe 60, Gln 111, Phe 113, and Trp 121) were correlated with previously reported binding site of Cyp-D where Cyclosporin-A was bound.³⁹ All the 20 novel molecules were docked as database into the predicted binding domain, and 30 conformations were generated for each molecule in the CypD binding site. Among them the conformation with the

lowest docking score was chosen to study the binding orientations of the ligands and each complex was assessed and ranked by the London ΔG energy scoring function.^{12,40}

Chemistry. Synthesis. General Procedure for the Synthesis of Compounds 4a–s. A solution of ethyl/methyl acetoacetate (1 mmol), urea/thiourea (1 mmol) and ethyl 2-(3-formyl-4-hydroxyphenyl)-4-methylthiazole-5-carboxylate (1 mmol) in ethanol (10 mL) was heated under reflux (78–80 °C) in the presence of polyphosphoric acid (3.3 mol %) for 12 h under an inert atmosphere. The progress of the reaction was monitored by TLC (hexane:ethyl acetate, 1:1 v/v). After being concentrated under vacuum at 50 °C, the reaction mixture was cooled to room temperature, poured into crushed ice (10 g), and stirred for 5–10 min. The solid that separated was filtered under reduced pressure and washed with ice-cold water (20 mL) before recrystallizing from hot ethanol to afford products 4a–s.

General Procedure for the Synthesis of Compounds 6a–s. To a solution of ethyl 6-methyl-4-(3-nitrophenyl)-2-thioxo-1,2,3,4-tetrahydropyrimidine-5-carboxylate (4a) (1 mmol) in ethyl acetate (5 mL), tetrahydrofuran (2.5 mL) and substituted 1-bromo-4-phenyl (1 mmol) were added to this solution, and the reaction mixture was refluxed for 8–12 h at room temperature. The progress of the reaction was monitored by thin layer chromatography (TLC; dichloromethane:ethylacetate 1:1). Solvent was then removed under reduced pressure to give the crude product which was recrystallized from methanol to give a pure product 6a. Related reactions were used to convert 4b–4s into 6b–6s. Compounds 6n, 6o, and 6p were synthesized according to our published paper and spectral data (IR, NMR, and HRMS) of previously known compounds were identical with those reported in the literature.⁴⁰

Synthesis of 2-(3-Cyano-4-isobutoxyphenyl)-4-methyl-N-(4-sulfamoylphenyl) Thiazole-5-carboxamide (9). A solution of 2-(3-cyano-4-isobutoxyphenyl)-4-methylthiazole-5-carboxylic acid (7) and thionyl chloride was stirred in dry toluene for 30 min in the presence of a catalytic amount of dimethylformamide. A clear solution resulted when the reaction temperature was slowly increased to 90–95 °C and continuously stirred for 3 h. Acid chloride formation was monitored by TLC (methylene dichloride:methanol 9:1). After completion, the reaction mixture was slowly cooled to room temperature and then concentrated at ambient temperature to give a white residue. This was dissolved in acetonitrile (20 mL), 4-aminobenzenesulfonamide (8) was added, and the solution was stirred for 4 h at 75 °C. This produced a solid that was separated by filtration, washed with acetonitrile (10 mL), and further washed with ice-cold water (10 mL) before recrystallizing from ethanol to afford pure compound 9.

Crystal Data and Structure Determination of the Synthesized Compound. Colorless single-domain crystals of ethyl 5-(4-hydroxyphenyl)-7-methyl-3-phenethyl-5H-thiazolo[3,2-a]pyrimidine-6-carboxylate (6n), ethyl 5-(4-fluorophenyl)-7-methyl-3-phenethyl-5H-thiazolo[3,2-a]pyrimidine-6-carboxylate (6o), and 2-(3-cyano-4-isobutoxyphenyl)-4-methyl-N-(4-sulfamoylphenyl) thiazole-5-carboxamide (9) suitable for single-crystal X-ray diffraction studies were grown from methanol. Crystallographic data and refinement results are summarized in Tables 3 and 4. Full hemispheres of redundant diffracted intensities were measured at 100(2) K for single-domain specimens of all three compounds using 2–6 s frames and ω - or ϕ -scan widths of 0.50°. Measurements were made with monochromated Cu K α radiation ($\lambda = 1.54178$ Å) on a

Bruker Proteum single crystal diffraction system having dual charge-coupled device (CCD) detectors sharing a Bruker MicroStar microfocus rotating anode X-ray source operating at 45 kV and 60 mA. Data for 6n and 6o were collected with a Platinum 135 CCD equipped with Helios high-brilliance multilayer optics and data for 9 were collected with an Apex II CCD detector equipped with Helios multilayer optics. Sample-to-detector distances of 80 mm (6o, 6p) and 50 mm (9) were used to collect data. Lattice constants for each crystal were determined with the Bruker SAINT software package using peak centers for 9843–9875 reflections. Integrated reflection intensities were produced for all structures using the Bruker program SAINT, and the data were corrected empirically for variable absorption effects using equivalent reflections. The Bruker software package SHELXTL was used to solve the structure using “direct methods” techniques. All stages of weighted full-matrix least-squares refinement were conducted using F_o^2 data with the SHELXTL v2010.3-0 software package.

The final structural models for all three structures incorporated anisotropic thermal parameters for all non-hydrogen atoms and isotropic thermal parameters for all hydrogen atoms. All hydrogen atoms for 6o and 6p were located in a difference Fourier and then included in the structural model as individual isotropic atoms whose parameters were allowed to vary in least-squares refinement cycles. Most of the hydrogen atoms for 9 were also located from a difference Fourier and included in the structural model as individual isotropic atoms whose parameters were allowed to vary in least-squares refinement cycles. The asymmetric unit for 9 contains two crystallographically independent molecules. The isopropyl group of the first molecule in 9 is disordered with two preferred orientations about the C(13)–C(14) bond. The minor (29%) orientation [atoms labeled with a prime (')] was restrained to have bond lengths and angles similar to the major (71%) orientation. When parameters for some of the hydrogen atoms in 9 refined to unreasonable values, they were fixed at idealized sp^2 - or sp^3 -hybridized positions and their isotropic thermal parameters were fixed at values equal to 1.20 (nonmethyl) or 1.50 (methyl) times the equivalent isotropic thermal parameter of the carbon atom to which they were covalently bonded. Five methyl groups for compound 9 were eventually incorporated into the final structural model as rigid groups (using idealized sp^3 -hybridized geometry and a C–H bond length of 0.98 Å) that were allowed to rotate freely about their C–C bonds in least-squares refinement cycles. Two hydrogens bonded to sp^2 -hybridized carbons and one bonded to an sp^3 -hybridized carbon were eventually placed at idealized positions with C–H bond lengths of 0.95 or 1.00 Å and isotropic thermal parameters fixed at values 1.20 times the equivalent isotropic thermal parameter of the carbon atom. The isotropic thermal parameter of H(48) was also fixed at a value 1.20 times the equivalent isotropic thermal parameter of C(48).

3. RESULTS AND DISCUSSION

Novel CypD Inhibitor Design. To create a novel drug for Alzheimer's treatment, multiple compounds were designed and synthesized and their capacity to inhibit CypD activity was predicted by QSAR and molecular docking studies. QSAR analysis has been used extensively as an aid in the design of novel and reactive molecules. Preliminary structure–activity relationship (SAR) studies revealed that the pyrimidine moiety is required for the inhibition of CypD activity and the presence

Table 1. Molecular Descriptors of Substituted Thiazolo[3,2-*a*]pyrimidine Derivatives (6a–s) and a Sulfonamide Derivative (9) from QSAR Study

comp no.	molecular weight	logS	atomic polarizability	radius of gyration	SlogP	molar refractivity	surface area	volume	logP(o/w)	density
6a	437.492	-5.195	62.933	3.808	4.051	11.840	228.972	394.500	4.464	0.801
6b	439.483	-5.852	62.021	3.835	4.485	11.669	190.875	391.625	4.925	0.813
6c	480.539	-5.822	67.651	3.738	4.868	12.309	141.269	412.625	4.894	0.775
6d	408.486	-4.746	61.031	3.763	3.222	11.507	201.689	379.125	3.917	0.772
6e	410.477	-5.403	60.119	3.765	3.655	11.336	150.986	377.875	4.378	0.784
6f	460.541	-6.056	66.416	3.799	4.133	12.288	159.793	409.750	4.856	0.739
6g	410.485	-4.810	60.786	3.763	4.395	11.274	208.095	380.000	4.598	0.782
6h	412.476	-5.467	59.874	3.761	4.828	11.103	157.814	378.750	5.059	0.794
6i	462.540	-6.120	66.171	3.806	5.306	12.055	158.940	407.375	5.537	0.747
6j	452.009	-5.164	67.488	4.018	2.765	12.603	241.371	423.500	3.604	0.791
6k	454.522	-5.304	67.243	3.911	3.174	12.330	186.172	413.625	4.307	0.804
6l	396.459	-4.419	57.937	3.717	2.832	11.045	222.368	364.375	3.576	0.782
6m	398.450	-5.076	57.025	3.693	3.265	10.874	179.439	360.000	4.037	0.794
6n	449.531	-6.433	66.984	4.155	5.461	12.499	189.877	419.750	5.725	0.771
6o	420.533	-5.281	65.749	4.071	5.258	12.000	144.647	407.375	5.482	0.741
6p	422.524	-5.938	64.837	4.079	5.692	11.830	95.952	404.375	5.943	0.752
6q	480.585	-4.899	73.540	4.235	3.860	13.154	204.436	452.625	4.414	0.761
6r	407.514	-4.724	63.322	4.098	3.601	11.721	182.292	394.125	4.060	0.746
6s	465.550	-5.142	69.780	4.285	3.145	12.817	216.144	434.375	3.747	0.767
9	470.574	-6.735	66.797	5.211	3.925	12.310	279.608	422.625	2.995	0.808

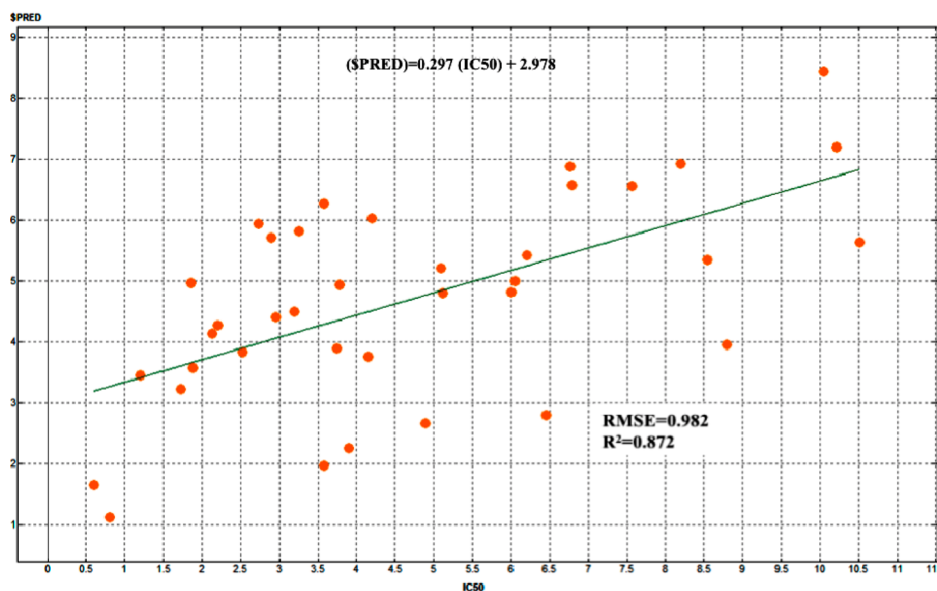


Figure 1. Linear correlation graph of measured IC_{50} values for 40 training set compounds with predicted values based on the calculated 2D QSAR model. The linearity of the trial set model is shown with the values of the error (RMSE) and correlation factor (R^2).

of *5H*-thiazolo-[3,2-*a*]pyrimidines provides the basic functionality necessary to achieve binding in the CypD active site. These studies are further validated by the fact that pyrimidine derivatives have also been widely used in the treatment of AD at various stages.^{41–44} In particular, pyrimidines have shown a remarkable ability to enhance permeation across biological membranes. Many derivatives have therefore been constructed and tested using virtual docking methods.⁴² The goal of our current research is to synthesize drugs that inhibit CypD activity and possibly provide enhanced viability by increasing the number of aromatic substituents on the basic pyrimidine and sulfonamide cores. *5H*-Thiazolo[3,2-*a*]pyrimidines were designed to incorporate significant intramolecular flexibility by linking polar groups having highly favorable enthalpic

interactions with conserved enzyme residues in the CypD binding site.

QSAR Study. Three-dimensional structures were built for all twenty test compounds (6a–s and 9) and optimized in the molecular operating environment (MOE). Molecular dynamics simulations were carried out for each compound individually and the stabilized conformations of the compounds were used to determine the molecular descriptors along with the application of Lipinski rule-of-five. Fifteen of the 20 molecules were predicted to have *superior* drug like properties, i.e. they satisfied all five Lipinski rules. The remaining five should have *excellent* drug-like properties since they satisfied four of the five Lipinski criteria; these five all had logP values between 5.06 and 5.94 (Table 1). The molecular descriptors of the present molecules are in optimal ranges with 15 of 20 compounds

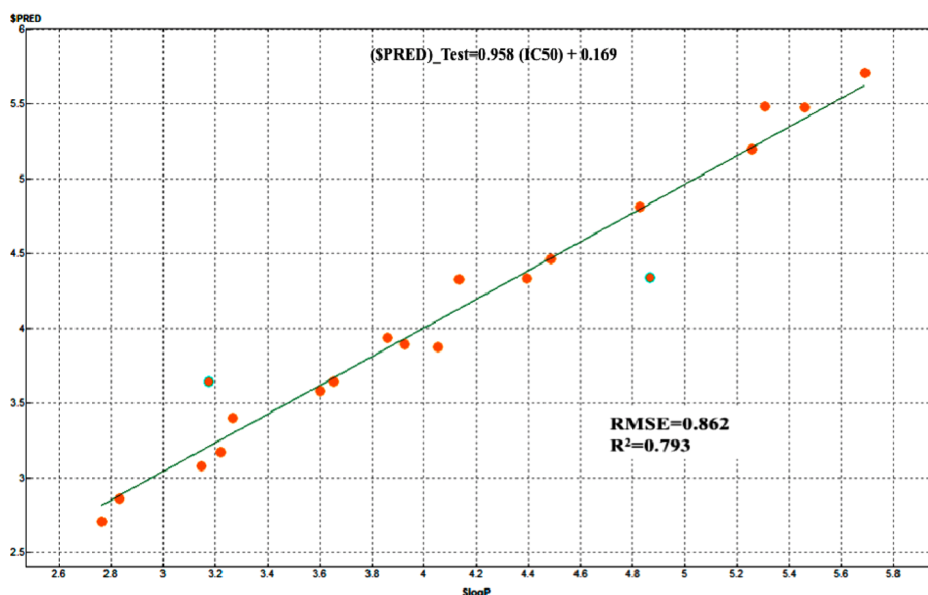


Figure 2. Linear correlation graph of measured IC_{50} values for 20 test set compounds with predicted values based on the calculated 2D QSAR model. The linearity of the trial set model is shown with the values of the error (RMSE) and correlation factor (R^2).

totally satisfying the Lipinski rule-of-five and the remaining 5 nearly satisfying the rules with LogP values that were slightly above the Lipinski limiting value of 5.00. A linear correlation plot resulted from the regression analysis for the *training* set of 40 compounds (Figure 1) when a single outlier was eliminated. The model exhibited excellent linearity [$SPRES = 0.297(IC_{50}) + 2.978$], with $RMSE = 0.982$ and $R^2 = 0.872$. The correlation plot for the QSAR model with the independent set of 20 newly designed test compounds was quite reasonable given the limited number of compounds in the training set. This was taken as an indication for the validity of applying the QSAR model. The resultant correlation regression analysis plot showed a perfect linear relationship for the final *test* data set [$SPRES = 0.958(IC_{50}) + 0.169$], with $RMSE = 0.862$ and $R^2 = 0.793$ (Figure 2).

A principal component analysis using the first three PCA eigenvectors included 98% of the variance. All the data values were found to lie in the range of -3 to $+3$. Each spot in the plot represents a molecule that is color coded by IC_{50} activity (Figure 3). This could provide an addition criterion for compound selection.

The pharmacophore model was derived for the test set compounds based on the specific features of the training set compounds. The test set compounds showed few similar and common pharmacophore features during the alignment. All of them are showing the common pharmacophore features like A1, A2, D6, R9, and R10 where the aromatic centers were matching to the maximum extent (Figure 4). This implies that the QSAR data is in very good correlation with the activity of training set molecules.

Molecular Docking. The ligand database that was developed from the total set of 20 test compounds that were used for docking with the known CypD receptor active site. Thirty ligand–receptor complex conformations were generated for each test compound, and the conformation with least docking score was considered for further analysis. The MOE interaction of all ligand molecules in the binding domain cavity was then analyzed by both London ΔG free energy approximations and ΔE interaction energies; this indicated

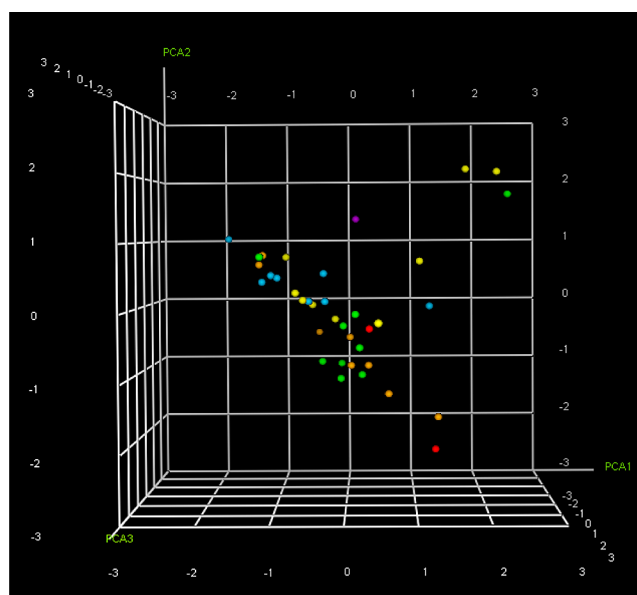


Figure 3. Plot of the principle component analysis (PCA) for the complete training set of 40 compounds. The first three principle eigenvectors are shown as PCA1, PCA2, and PCA3, and they constituted 98% of the variance. Coordinates for each of the 40 training compounds are indicated by a colored sphere.

that 10 of the 20 compounds should be ideal ligands. All 10 of these ligands (compounds **6e**, **6f**, **6h**, **6i**, **6k**, **6l**, **6n**, **6o**, **6p**, and **9**) exhibited good docking scores that were dominated by hydrogen bonding and salt-bridge formations with the binding domain of CypD (Table 2 and Figures 5–7). Hydrophobic interactions were also observed to play a contributing role. These docking experiments indicated that the molecules are good enough to act as CypD inhibitors. Among all docking conformations, compounds **6e** and **6n** had the best least docking scores of -12.891 and -12.294 kcal/mol, respectively. Compounds **6f**, **6p**, and **9** had the next best least docking scores with values for docking scores of -11.363 , -11.134 , and

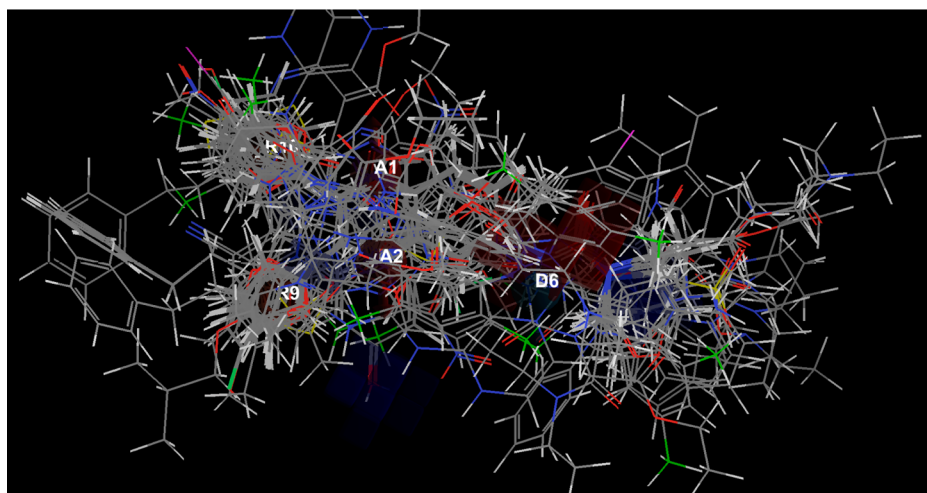


Figure 4. CypD pharmacophore model composed of the hydrophobic regions (Hyd) and H-bond donor/acceptor (Don&Acc). All the compounds are shown superimposed as occupying all four regions of the model.

Table 2. Molecular Docking Interaction of 20 Trial Compounds against the CypD (2BIT) Active Site

compd no ^a	docking score (kcal/mol) ^b	number of hydrogen bonds ^c	interacting residues of 2BIT ^d
6a	-9.040	3	His 54, Val 56, Gln 63
6b	-8.505	arene-cationic/ π interaction	Arg 55
6c	-8.640	—	—
6d	-9.150	2	His 54, Gly 150
6e	12.891	2	His 54, Gly 150
6f	-11.363	2	Gln 63, Asn 102
6g	-8.723	3	Arg 151, Thr 152, Thr 152
6h	-10.014	1	Arg 151
6i	-9.529	—	—
6j	-11.134	2	Phe 53, Thr 152
6k	-9.619	—	—
6l	-9.206	1	Arg 151
6m	-10.294	2	Thr 152, Thr 152
6n	-10.363	3	Arg 151, Ser 149, Arg 55
6o	-10.074	arene-H interaction	Arg 82, His 54
6p	-11.134	arene-arene interaction	His 54
6q	-8.314	arene-cationic π -interaction	Arg 151
6r	-8.095	1	Arg 151
6s	-9.332	1	Arg 55
9	-11.074	3, arene-arene π -interaction	His 54, Lys 155, Asn 71

^aThe novel CypD inhibitors. ^bDocking scores generated during MOE docking between the novel leads and CypD binding domain. ^cNumber of hydrogen bonds formed between the CypD binding domain and the novel leads. ^dThe interacting active site residues of CypD protein with the novel inhibitors in the ligand-receptor complex.

-11.074, respectively. Compound 9 was found to form an arene-arene π -stacking interaction with His 54.

Chemistry. On the basis of QSAR, pharmacophore modeling and molecular docking studies, 10 compounds (6e, 6f, 6h, 6i, 6k, 6l, 6n, 6o, 6p, and 9) were selected for synthesis. Nine are pyrimidine derivatives, and the tenth is a sulfonamide derivative. These compounds were shown to have the best

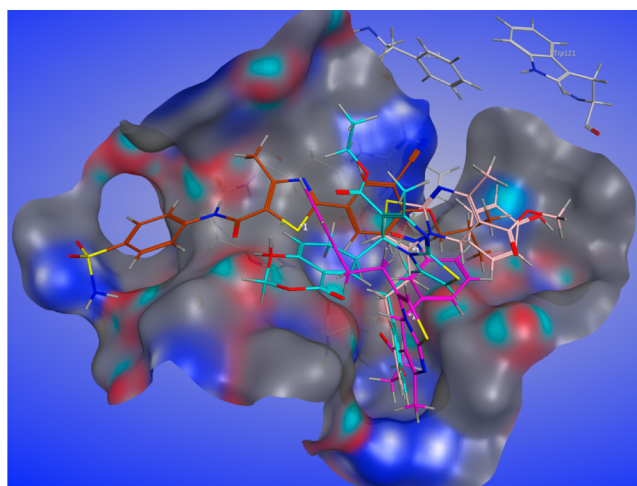


Figure 5. Compounds 6f, 6o, 6p, and 9 are shown in their docked position within the 2BIT structure. The active site regions are indicated. The enzymatic triads are shown relative to the docked potential candidates.

interactions with the CypD active site. They gave the lowest docking scores among all compounds considered and showed satisfactory QSAR and drug-like properties. These pyrimidine derivatives were all synthesized in refluxing ethanol by reacting aromatic aldehydes (1), methyl/ethyl acetoacetate (2), and thiourea (3) in the presence of polyphosphoric acid (PPA) (3.3 mol %) for 8–12 h to yield dihydropyrimidine derivatives 4e, 4f, 4h, 4i, 4k, 4l, 4n, 4o, and 4p. Reaction progress was monitored by TLC (dichloromethane:ethyl acetate, 1:1 v/v). Spectral data (IR, NMR, and HRMS) of previously known compounds were identical with those reported in the literature. The intermediate dihydropyrimidines 4e, 4f, 4h, 4i, 4k, 4l, 4n, 4o, and 4p were reacted with substituted aromatic 1-bromo compounds at reflux temperature for 6–12 h to obtain our target CypD inhibitors 6e, 6f, 6h, 6i, 6k, 6l, 6n, 6o, and 6p as shown in Scheme 1 and Table 3. The chemical structures of the new compounds were confirmed by IR, ¹H NMR, ¹³C NMR spectral, and HRMS; the spectral data are provided in the Supporting Information. Structures for compounds 6o (Figure 8 and Table 4) and 6p (Figure 9 and Table 4) were further confirmed by single-crystal XRD.

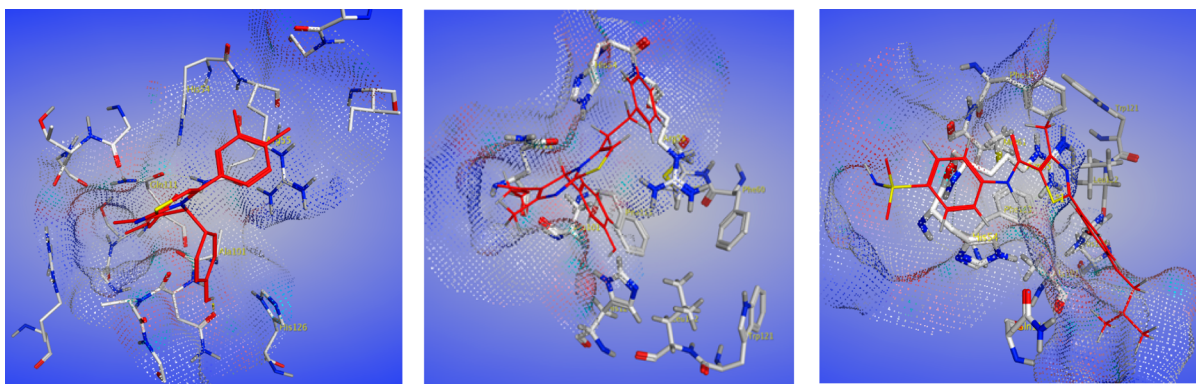


Figure 6. Binding site for active IC₅₀ compounds **6f**, **6o**, and **9**. Two H-bonds to Asn 102 and Gln 63 make major contributions to the binding affinity for compound **6f** (left). Salt bridges to Lys 152 and Asn 71 and an H-bond to His 54 make major contributions to the binding affinity for compound **9** (right); H-bonding interactions and salt bridges are shown with dotted lines. The arene–arene π -stacking interaction between His 54 and H-bonding with Arg 82 compound **6o** is shown on the middle.

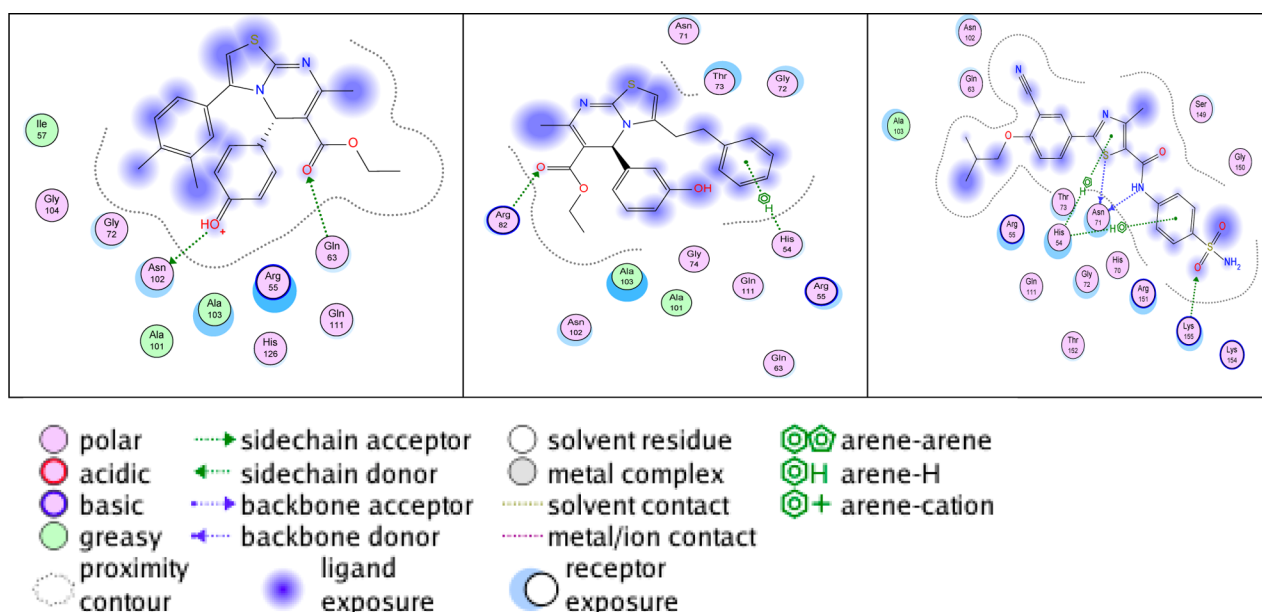
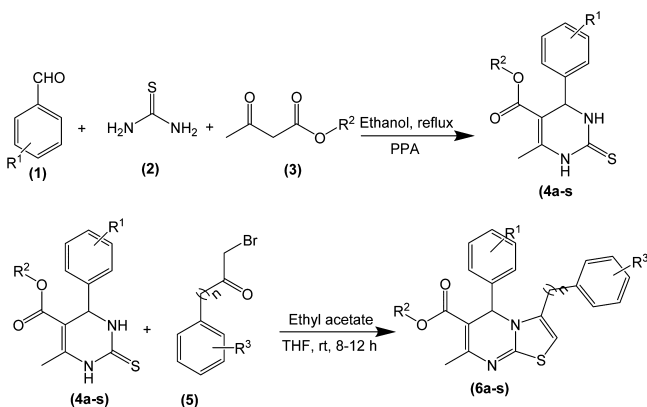


Figure 7. 2D Ligand interaction maps of compound **6f** (left), compound **6o** (middle), and compound **9** (right) binding to CypD.

Scheme 1. Synthetic Route for Small Molecule Pyrimidine Inhibitors of Human CypD



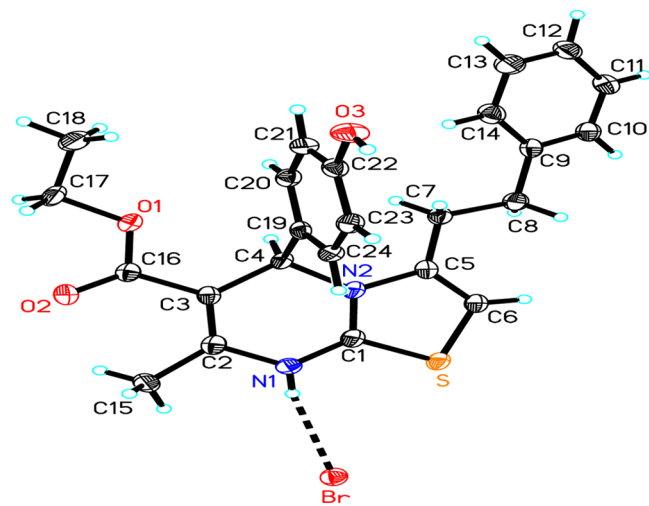
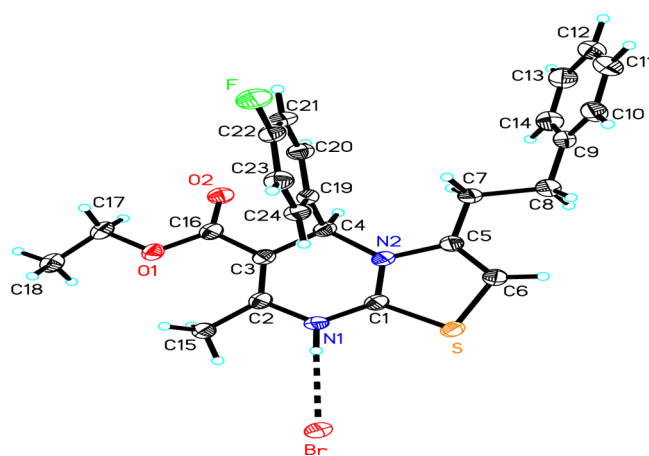
Sulfonamide (**9**) was prepared by the reaction of Febuxostat (**7**) with thionyl chloride in the presence of a catalytic amount of *N,N*-dimethylformamide. The thionyl chloride reacted with **7** to form the corresponding acid chloride that then reacted

with substituted 4-aminobenzenesulfonamide, in the presence of triethylamine in toluene, to give the corresponding sulfonamide derivative 2-(3-cyano-4-isobutoxyphenyl)-4-methyl-*N*-(4-sulfamoylphenyl)thiazole-5-carboxamide (**9**) (Scheme 2). The progress of the reaction was monitored by TLC (dichloromethane:ethyl acetate 1:1 v/v). The chemical structure of the new compound was confirmed by elemental analysis, IR, ¹H NMR, ¹³C NMR, and HRMS; the spectral data are provided in the Supporting Information. The structure of compound **9** (Figure 10 and Table 5) was further confirmed by single crystal XRD.

Crystal Data and Structure Determination of the Synthesized Compounds. Pyrimidine derivatives **6o** and **6p** and sulfonamide derivative **9** were each recrystallized from methanol to give colorless crystals suitable for single-crystal X-ray diffraction experiments. Crystallographic data are summarized in Table 3 for **6o** and **6p** and in Table 4 for **9**. The intensity data were collected at 100(2) K using monochromatic Cu $K\alpha$ radiation ($\lambda = 1.54178 \text{ \AA}$) radiation on Bruker Proteum diffractometer that has two CCD detectors sharing a Bruker MicroStar microfocus rotating anode X-ray source operating at

Table 3. Representative Compounds

entry	R	R ¹	R ²	n	entry	R	R ¹	R ²	n
6a	3-NO ₂	4-OH	ethyl	1	6k	4-OH, SOOCH ₃	4-F	ethyl	1
6b	3-NO ₂	4-F	ethyl	1	6l	4-OH	4-OH	methyl	1
6c	3-NO ₂	3,4-di chloro	ethyl	1	6m	4-OH	4-F	methyl	1
6d	4-OH	4-OH	ethyl	1	6n	3-NO ₂	–	ethyl	2
6e	4-OH	4-F	ethyl	1	6o	4-OH	–	ethyl	2
6f	4-OH	3,4-di chloro	ethyl	1	6p	4-F	–	ethyl	2
6g	4-F	4-OH	ethyl	1	6q	4-OH, SOOCH ₃	–	ethyl	2
6h	4-F	4-F	ethyl	1	6r	4-OH	–	methyl	2
6i	4-F	3,4-di chloro	ethyl	1	6s	4-OH, SOOCH ₃	–	methyl	2
6j	4-OH, SOOCH ₃	4-OH	methyl	1					

Figure 8. Crystal structure for HBr salt of **6o** showing 50% probability displacement ellipsoids and atom-numbering scheme.Figure 9. Crystal structure for HBr salt of **6p** showing 50% probability displacement ellipsoids and atom-numbering scheme.

45 mA and 60 kV. Nearly complete (98.3–99.6% to $\theta = 66.00^\circ$) redundant sets of unique data for **6o** and **6p** were collected with a Platinum 135 CCD detector equipped with Helios high-brilliance multilayer optics; similar data for **9** were collected with an Apex II CCD detector equipped with Helios multilayer optics. A crystal-to-detector distance of 80 mm was used for **6o** and **6p**, and a crystal-to-detector distance of 50 mm was used for **9**. The intensity data were processed using the Bruker suite of data processing programs (SAINT), and absorption corrections were applied using SADABS. The

Table 4. Crystal Data and Details of the Structure Determination for **6o** and **6p**

identification code	6o	6p
empirical formula	C ₂₄ H ₂₅ BrN ₂ O ₄ S	C ₂₄ H ₂₄ BrF N ₂ O ₂ S
formula weight	517.43	503.42
temperature	100(2) K	100(2) K
wavelength	1.54178 Å	1.54178 Å
crystal system	monoclinic	monoclinic
space group	P2 ₁ /c	P2 ₁ /c
unit cell dimensions	$a = 6.5365(7)$ Å $\alpha = 90^\circ$	$a = 14.7445(16)$ Å $\alpha = 90.000^\circ$
	$b = 18.132(2)$ Å $\beta = 95.327(2)^\circ$	$b = 6.8046(7)$ Å $\beta = 98.128(2)^\circ$
	$c = 18.855(2)$ Å $\lambda = 90.000^\circ$	$c = 22.826(2)$ Å $\lambda = 90.000^\circ$
volume	2224.9(4) Å ³	2267.1(4) Å ³
Z	4	4
density (calculated)	1.545 g/cm ³	1.475 g/cm ³
absorption coefficient	3.687 mm ⁻¹	3.598 mm ⁻¹
F(000)	1064	1032
crystal size	0.42 × 0.08 × 0.06 mm ³	0.17 × 0.06 × 0.03 mm ³
theta range for data collection	3.39–67.89°	6.79–67.90°
index ranges	$-7 \leq h \leq 6, -21 \leq k \leq 21, -22 \leq l \leq 22$	$-17 \leq h \leq 17, -7 \leq k \leq 7, -22 \leq l \leq 27$
reflections collected	13265	12782
independent reflections	3921 [$R_{\text{int}} = 0.026$]	3934 [$R_{\text{int}} = 0.029$]
completeness to theta = 66.00°	98.8%	98.3%
absorption correction	multiscan	multiscan
max. and min transmission	1.000 and 0.594	1.000 and 0.778
refinement method	full-matrix least-squares on F^2	full-matrix least-squares on F^2
data/restraints/parameters	3921/0/381	3934/0/377
goodness-of-fit on F^2	1.085	1.065
final R indices [$I > 2\sigma(I)$]	$R_1 = 0.027, wR_2 = 0.075$	$R_1 = 0.027, wR_2 = 0.069$
R indices (all data)	$R_1 = 0.027, wR_2 = 0.075$	$R_1 = 0.028, wR_2 = 0.070$
largest diff. peak and hole	0.47 and -0.44 e ⁻ /Å ³	0.36 and -0.46 e ⁻ /Å ³

crystal structures were solved by direct methods and refined by full matrix least-squares refinement on F^2 using SHELXL. Nonhydrogen atoms were modeled with anisotropic thermal parameters and hydrogen atoms were modeled with isotropic

Scheme 2. Synthetic Route for Small Molecule Sulfonamide Inhibitor of Human CypD

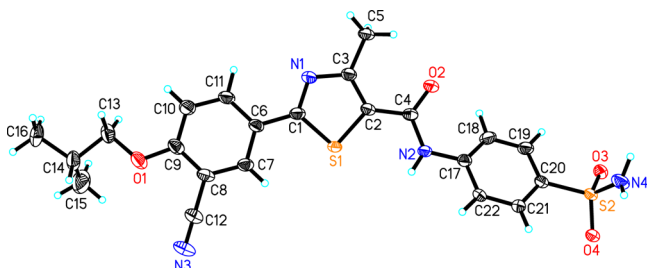
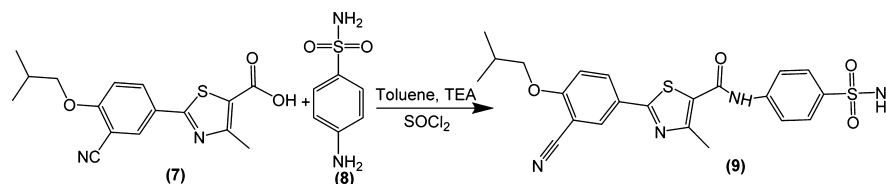


Figure 10. Crystal structure for compound 9 showing 50% probability displacement ellipsoids and atom-numbering scheme.

Table 5. Crystal Data and Details of the Structure Determination for Compound 9

identification code	9
empirical formula	C ₄₄ H ₄₄ N ₈ O ₈ S ₄
formula weight	941.11
temperature	100(2) K
wavelength	1.54178 Å
crystal system	monoclinic
space group	P2 ₁ /c
unit cell dimensions	$a = 17.0482(4)$ Å $\alpha = 90^\circ$ $b = 14.1161(4)$ Å $\beta = 113.516(1)^\circ$ $c = 19.9664(5)$ Å $\lambda = 90^\circ$
volume	4405.9(2) Å ³
Z	4
density (calculated)	1.419 g/cm ³
absorption coefficient	2.513 mm ⁻¹
F(000)	1968
crystal size	0.11 × 0.10 × 0.10 mm ³
theta range for data collection	2.83–69.85°
index ranges	–20 ≤ h ≤ 19, –17 ≤ k ≤ 16, –24 ≤ l ≤ 24
reflections collected	37842
independent reflections	8157 [R _{int} = 0.029]
completeness to theta = 66.00°	99.6%
absorption correction	multiscan
max and min transmission	1.000 and 0.895
refinement method	full-matrix least-squares on F ²
data/restraints/parameters	8157/9/741
goodness-of-fit on F ²	1.055
final R indices [I > 2sigma(I)]	R ₁ = 0.057, wR ₂ = 0.156
R indices (all data)	R ₁ = 0.060, wR ₂ = 0.159
largest diff. peak and hole	0.98 and –0.72 e ⁻ /Å ³

thermal parameters. All of the hydrogen atoms for **6o** and **6p** and most of the hydrogen atoms for **9** were refined as independent isotropic atoms after being located from difference Fourier. The remaining hydrogen atoms for **9** were fixed at idealized positions.

4. CONCLUSION AND FUTURE DIRECTION

In this study, we report the design, synthesis, docking, 2D QSAR, and pharmacophore studies for a series of 20 CypD

inhibitors, 10 of which were synthesized. Single crystal X-ray structures are reported for three of these. Our molecules exhibited strong binding affinity with the CypD receptor during the molecular docking process. 2D QSAR and 3D pharmacophore studies have been used as tools for selecting active drug candidates from a large volume of prospective compounds designed to incorporate desirable structural features. We hope these results demonstrate the ability of these procedures to accurately predict active drug candidates. The docking, 2D QSAR, and pharmacophore studies indicate that 10 (**6e**, **6f**, **6h**, **6i**, **6k**, **6l**, **6n**, **6o**, **6p**, and **9**) of the 20 candidate compounds should be superior inhibitors of CypD. We hope to use and refine this as an effective strategy for developing even more potent CypD inhibitors for use in treating Alzheimer's disease.

■ ASSOCIATED CONTENT

Supporting Information

Spectroscopic data for synthesized compounds (¹H, ¹³C, NMR, HRMS), interaction of remaining 17 novel inhibitors with CypD active site and detailed crystallographic experimental details with structural tables. This material is available free of charge via the Internet at <http://pubs.acs.org>.

■ AUTHOR INFORMATION

Corresponding Author

*Mailing address: 2099 Constant Avenue, University of Kansas, Lawrence, KS 66047. E-mail: shidu@ku.edu.

Notes

The authors declare no competing financial interest.

■ ACKNOWLEDGMENTS

This study was supported by grant awards (R37AG037319, R01GM095355, and RO1NS NS65482) from the National Institute of General Medical Sciences and the National Institute on Aging. The authors thank the National Science Foundation (grant CHE-0923449) and the University of Kansas for funds to purchase the x-ray instrumentation and computers.

■ ABBREVIATIONS

CypD, Cyclophilin D; mPTP, mitochondrial membrane permeability transition pore; ACh, acetylcholine; AD, Alzheimer's disease; SPR, surface plasmon resonance; Aβ, amyloid beta; QSAR, quantitative structure–activity relationship; BBB, blood–brain barrier; SAR, structure–activity relationship; CNS, central nervous system; MOE, molecular operating environment; RMSE, root mean square error; PCA, principle component analysis; PDB, protein data bank; MMFF94x, the Merck molecular force field

■ REFERENCES

- (1) Caspersen, C.; Wang, N.; Yao, J.; Sosunov, A.; Chen, X.; Lustbader, J. W.; Xu, H. W.; Stern, D.; McKhann, G.; Yan, S. D. Mitochondrial Abeta: a potential focal point for neuronal metabolic dysfunction in Alzheimer's disease. *FASEB J.* **2005**, *19*, 2040–1.

- (2) Reddy, P. H.; Beal, M. F. Amyloid beta, mitochondrial dysfunction and synaptic damage: implications for cognitive decline in aging and Alzheimer's disease. *Trends in Mol. Med.* **2008**, *14*, 45–53.
- (3) Du, H.; Guo, L.; Yan, S.; Sosunov, A. A.; McKhann, G. M.; Yan, S. S. Early deficits in synaptic mitochondria in an Alzheimer's disease mouse model. *Proc. Natl. Acad. Sci. USA* **2010**, *107*, 18670–5.
- (4) Lunnnon, K.; Ibrahim, Z.; Proitsi, P.; Lourdasamy, A.; Newhouse, S.; Sattlecker, M.; Furney, S.; Saleem, M.; Soininen, H.; Kloszewska, I.; Mecocci, P.; Tsolaki, M.; Vellas, B.; Coppola, G.; Geschwind, D.; Simmons, A.; Lovestone, S.; Dobson, R.; Hodges, A.; AddNeuroMed, C. Mitochondrial dysfunction and immune activation are detectable in early Alzheimer's disease blood. *J. Alzheimer's Disease: JAD* **2012**, *30*, 685–710.
- (5) Valasani, K. R.; Sun, Q.; Hu, G.; Li, J.; Du, F.; Guo, Y.; Carlson, E. A.; Gan, X.; Yan, S. S. Identification of Human ABAD Inhibitors for Rescuing Abeta-Mediated Mitochondrial Dysfunction. *Curr. Alzheimer Res.* **2014**, DOI: 10.2174/1567205011666140130150108.
- (6) Du, H.; Guo, L.; Fang, F.; Chen, D.; Sosunov, A. A.; McKhann, G. M.; Yan, Y.; Wang, C.; Zhang, H.; Molkentin, J. D.; Gunn-Moore, F. J.; Vonsattel, J. P.; Arancio, O.; Chen, J. X.; Yan, S. D. Cyclophilin D deficiency attenuates mitochondrial and neuronal perturbation and ameliorates learning and memory in Alzheimer's disease. *Nature Med.* **2008**, *14*, 1097–105.
- (7) Manczak, M.; Anekonda, T. S.; Henson, E.; Park, B. S.; Quinn, J.; Reddy, P. H. Mitochondria are a direct site of A beta accumulation in Alzheimer's disease neurons: implications for free radical generation and oxidative damage in disease progression. *Human Mol. Genetics* **2006**, *15*, 1437–49.
- (8) Lustbader, J. W.; Cirilli, M.; Lin, C.; Xu, H. W.; Takuma, K.; Wang, N.; Caspersen, C.; Chen, X.; Pollak, S.; Chaney, M.; Trinchese, F.; Liu, S.; Gunn-Moore, F.; Lue, L. F.; Walker, D. G.; Kuppasamy, P.; Zewier, Z. L.; Arancio, O.; Stern, D.; Yan, S. S.; Wu, H. ABAD directly links Abeta to mitochondrial toxicity in Alzheimer's disease. *Science* **2004**, *304*, 448–52.
- (9) Hauptmann, S.; Scherping, I.; Drose, S.; Brandt, U.; Schulz, K. L.; Jendrach, M.; Leuner, K.; Eckert, A.; Muller, W. E. Mitochondrial dysfunction: an early event in Alzheimer pathology accumulates with age in AD transgenic mice. *Neurobiol. Aging* **2009**, *30*, 1574–86.
- (10) Yao, J.; Irwin, R. W.; Zhao, L.; Nilsen, J.; Hamilton, R. T.; Brinton, R. D. Mitochondrial bioenergetic deficit precedes Alzheimer's pathology in female mouse model of Alzheimer's disease. *Proc. Natl. Acad. Sci. USA* **2009**, *106*, 14670–5.
- (11) Yan, S. D.; Fu, J.; Soto, C.; Chen, X.; Zhu, H.; Al-Mohanna, F.; Collison, K.; Zhu, A.; Stern, E.; Saido, T.; Tohyama, M.; Ogawa, S.; Roher, A.; Stern, D. An intracellular protein that binds amyloid-beta peptide and mediates neurotoxicity in Alzheimer's disease. *Nature* **1997**, *389*, 689–95.
- (12) Valasani, K. R.; Hu, G.; Chaney, M. O.; Yan, S. S. Structure-Based Design and Synthesis of Benzothiazole Phosphonate Analogues with Inhibitors of Human ABAD-A beta for Treatment of Alzheimer's Disease. *Chem. Biol. Drug Des.* **2013**, *81*, 238–249.
- (13) Stains, C. L.; Mondal, K.; Ghosh, I. Molecules that target beta-amyloid. *ChemMedChem* **2007**, *2*, 1674–92.
- (14) Ghosh, A. K.; Venkateswara Rao, K.; Yadav, N. D.; Anderson, D. D.; Gavande, N.; Huang, X.; Terzyan, S.; Tang, J. Structure-Based Design of Highly Selective beta-Secretase Inhibitors: Synthesis, Biological Evaluation, and Protein-Ligand X-ray Crystal Structure. *J. Med. Chem.* **2012**, *55*, 9195–207.
- (15) Gravenfors, Y.; Viklund, J.; Blid, J.; Ginman, T.; Karlstrom, S.; Kihlstrom, J.; Kolmodin, K.; Lindstrom, J.; von Berg, S.; von Kieseritzky, F.; Bogar, K.; Slivo, C.; Swahn, B. M.; Olsson, L. L.; Johansson, P.; Eketjall, S.; Falting, J.; Jeppsson, F.; Stromberg, K.; Janson, J.; Rahm, F. Correction to New Aminoimidazoles as beta-Secretase (BACE-1) Inhibitors Showing Amyloid-beta (Abeta) Lowering in Brain. *J. Med. Chem.* **2012**, *55*, 9297–9311.
- (16) Ogura, A.; Morizane, A.; Nakajima, Y.; Miyamoto, S.; Takahashi, J. gamma-Secretase Inhibitors Prevent Overgrowth of Transplanted Neural Progenitors Derived from Human-Induced Pluripotent Stem Cells. *Stem Cells Dev.* **2013**, *22*, 374–382.
- (17) Parker, M. F.; Barten, D. M.; Bergstrom, C. P.; Bronson, J. J.; Corsa, J. A.; Dee, M. F.; Gai, Y.; Guss, V. L.; Higgins, M. A.; Keavy, D. J.; Loo, A.; Mate, R. A.; Marcin, L. R.; McElhone, K. E.; Polson, C. T.; Roberts, S. B.; Macor, J. E. 2-(N-Benzyl-N-phenylsulfonamido)alkyl amide derivatives as gamma-secretase inhibitors. *Bioorg. Med. Chem. Lett.* **2012**, *22*, 6828–6831.
- (18) Ozudogru, S. N.; Lippa, C. F. Disease modifying drugs targeting beta-amyloid. *Am. J. Alzheimer's Disease Other Dementias* **2012**, *27*, 296–300.
- (19) Panza, F.; Solfrizzi, V.; Frisardi, V.; Imbimbo, B. P.; Capurso, C.; D'Introno, A.; Colacicco, A. M.; Seripa, D.; Vendemiale, G.; Capurso, A.; Pilotto, A. Beyond the neurotransmitter-focused approach in treating Alzheimer's disease: drugs targeting beta-amyloid and tau protein. *Aging Clin. Exp. Res.* **2009**, *21*, 386–406.
- (20) Frisardi, V.; Solfrizzi, V.; Imbimbo, P. B.; Capurso, C.; D'Introno, A.; Colacicco, A. M.; Vendemiale, G.; Seripa, D.; Pilotto, A.; Capurso, A.; Panza, F. Towards disease-modifying treatment of Alzheimer's disease: drugs targeting beta-amyloid. *Curr. Alzheimer Res.* **2010**, *7*, 40–55.
- (21) Orlando, R. A.; Gonzales, A. M.; Royer, R. E.; Deck, L. M.; Vander Jagt, D. L. A chemical analog of curcumin as an improved inhibitor of amyloid Abeta oligomerization. *PLoS One* **2012**, *7*, e31869.
- (22) Park, S. K.; Pegan, S. D.; Mesecar, A. D.; Jungbauer, L. M.; LaDu, M. J.; Liebman, S. W. Development and validation of a yeast high-throughput screen for inhibitors of Abeta(4)(2) oligomerization. *Disease Models Mech.* **2011**, *4*, 822–831.
- (23) Walsh, D. M.; Townsend, M.; Podlisny, M. B.; Shankar, G. M.; Fadeeva, J. V.; El Agnaf, O.; Hartley, D. M.; Selkoe, D. J. Certain inhibitors of synthetic amyloid beta-peptide (Abeta) fibrillogenesis block oligomerization of natural Abeta and thereby rescue long-term potentiation. *J. Neurosci.* **2005**, *25*, 2455–2462.
- (24) Du, H.; Guo, L.; Zhang, W.; Rydzewska, M.; Yan, S. Cyclophilin D deficiency improves mitochondrial function and learning/memory in aging Alzheimer disease mouse model. *Neurobiol. Aging* **2011**, *32*, 398–406.
- (25) Takuma, K.; Yao, J.; Huang, J.; Xu, H.; Chen, X.; Luddy, J.; Trillat, A. C.; Stern, D. M.; Arancio, O.; Yan, S. S. ABAD enhances Abeta-induced cell stress via mitochondrial dysfunction. *FASEB J.* **2005**, *19*, 597–598.
- (26) Tanveer, A.; Virji, S.; Andreeva, L.; Totty, N. F.; Hsuan, J. J.; Ward, J. M.; Crompton, M. Involvement of cyclophilin D in the activation of a mitochondrial pore by Ca²⁺ and oxidant stress. *Eur. J. Biochem./FEBS* **1996**, *238*, 166–172.
- (27) Griffiths, E. J.; Halestrap, A. P. Further evidence that cyclosporin A protects mitochondria from calcium overload by inhibiting a matrix peptidyl-prolyl cis-trans isomerase. Implications for the immunosuppressive and toxic effects of cyclosporin. *Biochem. J.* **1991**, *274* (Pt 2), 611–614.
- (28) Galat, A.; Metcalfe, S. M. Peptidylproline cis/trans isomerases. *Progress Biophys. Molec. Biol.* **1995**, *63*, 67–118.
- (29) Khaspekov, L.; Friberg, H.; Halestrap, A.; Viktorov, I.; Wieloch, T. Cyclosporin A and its nonimmunosuppressive analogue N-Me-Val-4-cyclosporin A mitigate glucose/oxygen deprivation-induced damage to rat cultured hippocampal neurons. *Eur. J. Neurosci.* **1999**, *11*, 3194–3198.
- (30) Nicolli, A.; Basso, E.; Petronilli, V.; Wenger, R. M.; Bernardi, P. Interactions of cyclophilin with the mitochondrial inner membrane and regulation of the permeability transition pore, and cyclosporin A-sensitive channel. *J. Biol. Chem.* **1996**, *271*, 2185–2192.
- (31) Clarke, S. J.; McStay, G. P.; Halestrap, A. P. Sanglifehrin A acts as a potent inhibitor of the mitochondrial permeability transition and reperfusion injury of the heart by binding to cyclophilin-D at a different site from cyclosporin A. *J. Biol. Chem.* **2002**, *277*, 34793–34799.
- (32) Azzolin, L.; Antolini, N.; Calderan, A.; Ruzza, P.; Sciacovelli, M.; Marin, O.; Mammi, S.; Bernardi, P.; Rasola, A. Antamanide, a derivative of Amanita phalloides, is a novel inhibitor of the mitochondrial permeability transition pore. *PLoS One* **2011**, *6*, e16280.

(33) Guo, H. X.; Wang, F.; Yu, K. Q.; Chen, J.; Bai, D. L.; Chen, K. X.; Shen, X.; Jiang, H. L. Novel cyclophilin D inhibitors derived from quinoxaline exhibit highly inhibitory activity against rat mitochondrial swelling and Ca²⁺ uptake/ release. *Acta Pharma. Sin.* **2005**, *26*, 1201–1211.

(34) Wang, F.; Chen, J.; Liu, X. J.; Shen, X.; He, X. C.; Jiang, H. L.; Bai, D. L. Synthesis and peptidyl-prolyl isomerase inhibitory activity of quinoxalines as ligands of cyclophilin A. *Chem. Pharm. Bull.* **2006**, *54*, 372–376.

(35) Guo, H. X.; Wang, F.; Yu, K. Q.; Chen, Y.; Bai, D. L.; Chen, K. X.; Shen, X.; Jiang, H. L. Novel cyclophilin D inhibitors derived from quinoxaline exhibit highly inhibitory activity against rat mitochondrial swelling and Ca²⁺ uptake/release. *Acta Pharma. Sin.* **2005**, *26*, 1201–1211.

(36) Li, J.; Chen, J.; Zhang, L.; Wang, F.; Gui, C. S.; Zhang, L.; Qin, Y.; Xu, Q.; Liu, H.; Nan, F. J.; Shen, J. K.; Bai, D. L.; Chen, K. X.; Shen, X.; Jiang, H. L. One novel quinoxaline derivative as a potent human cyclophilin A inhibitor shows highly inhibitory activity against mouse spleen cell proliferation. *Bioorg. Med. Chem.* **2006**, *14*, 5527–5534.

(37) Vilar, S.; Cozza, G.; Moro, S. Medicinal Chemistry and the Molecular Operating Environment (MOE): Application of QSAR and Molecular Docking to Drug Discovery. *Curr. Top Med. Chem.* **2008**, *8*, 1555–1572.

(38) Vilar, S.; Gonzalez-Diaz, H.; Santana, L.; Uriarte, E. QSAR model for alignment-free prediction of human breast cancer biomarkers based on electrostatic potentials of protein pseudofolding HP-lattice networks. *J. Comput. Chem.* **2008**, *29*, 2613–2622.

(39) Kajitani, K.; Fujihashi, M.; Kobayashi, Y.; Shimizu, S.; Tsujimoto, Y.; Miki, K. Crystal structure of human cyclophilin D in complex with its inhibitor, cyclosporin A at 0.96-Å resolution. *Proteins* **2008**, *70*, 1635–1639.

(40) Valasani, K. R.; Chaney, M. O.; Day, V. W.; Yan, S. S. Acetylcholinesterase Inhibitors: Structure Based Design, Synthesis, Pharmacophore Modeling, and Virtual Screening. *J. Chem. Inf. Model.* **2013**, *53*, 2033–2046.

(41) Zhi, H.; Chen, L. M.; Zhang, L. L.; Liu, S. J.; Wan, D. C. C.; Lin, H. Q.; Hu, C. Design, synthesis, and biological evaluation of 5H-thiazolo[3,2-a]pyrimidine derivatives as a new type of acetylcholinesterase inhibitors. *Arkivoc* **2008**, 266–277.

(42) Rivkin, A.; Ahearn, S. P.; Chichetti, S. M.; Kim, Y. R.; Li, C. M.; Rosenau, A.; Kattar, S. D.; Jung, J.; Shah, S.; Hughes, B. L.; Crispino, J. L.; Middleton, R. E.; Szewczak, A. A.; Munoz, B.; Shearman, M. S. Piperazinyl pyrimidine derivatives as potent gamma-secretase modulators. *Bioorg. Med. Chem. Lett.* **2010**, *20*, 1269–1271.

(43) Messer, W. S., Jr.; Rajeswaran, W. G.; Cao, Y.; Zhang, H. J.; el-Assadi, A. A.; Dockery, C.; Liske, J.; O'Brien, J.; Williams, F. E.; Huang, X. P.; Wroblewski, M. E.; Nagy, P. I.; Peseckis, S. M. Design and development of selective muscarinic agonists for the treatment of Alzheimer's disease: characterization of tetrahydropyrimidine derivatives and development of new approaches for improved affinity and selectivity for M1 receptors. *Pharma. Acta Helvetiae* **2000**, *74*, 135–40.

(44) Kypta, R. M. GSK-3 inhibitors and their potential in the treatment of Alzheimer's disease. *Expert Opin. Ther. Pat.* **2005**, *15*, 1315–1331.